Basics of Plume Impingement Analysis for Small Chemical and Cold Gas Thrusters

Georg Dettleff* Martin Grabe*

January 27, 2011

Contents

*DLR Göttingen, Institute of Aerodynamics and Flow Technology, Spacecraft Section, 37073 Göttingen, Germany

Report Documentation Page

Form Approved
OMB No. 0704-0188

1. REPORT DATE	2. REPORT TYPE	3. DATES COVERED
JAN 2011	**N/A**	**-**

4. TITLE AND SUBTITLE	5a. CONTRACT NUMBER
Basics of Plume Impingement Analysis for Small Chemical and Cold Gas Thrusters	5b. GRANT NUMBER
	5c. PROGRAM ELEMENT NUMBER
6. AUTHOR(S)	5d. PROJECT NUMBER
	5e. TASK NUMBER
	5f. WORK UNIT NUMBER
7. PERFORMING ORGANIZATION NAME(S) AND ADDRESS(ES) **DLR Göttingen, Institute of Aerodynamics and Flow Technology, Spacecraft Section, 37073 Göttingen, Germany**	8. PERFORMING ORGANIZATION REPORT NUMBER
9. SPONSORING/MONITORING AGENCY NAME(S) AND ADDRESS(ES)	10. SPONSOR/MONITOR'S ACRONYM(S)
	11. SPONSOR/MONITOR'S REPORT NUMBER(S)

12. DISTRIBUTION/AVAILABILITY STATEMENT
Approved for public release, distribution unlimited

13. SUPPLEMENTARY NOTES
See also ADA579248. Models and Computational Methods for Rarefied Flows (Modeles et methodes de calcul des coulements de gaz rarefies). RTO-EN-AVT-194

14. ABSTRACT

15. SUBJECT TERMS

16. SECURITY CLASSIFICATION OF:			17. LIMITATION OF ABSTRACT	18. NUMBER OF PAGES	19a. NAME OF RESPONSIBLE PERSON
a. REPORT	b. ABSTRACT	c. THIS PAGE			
unclassified	**unclassified**	**unclassified**	**SAR**	**40**	

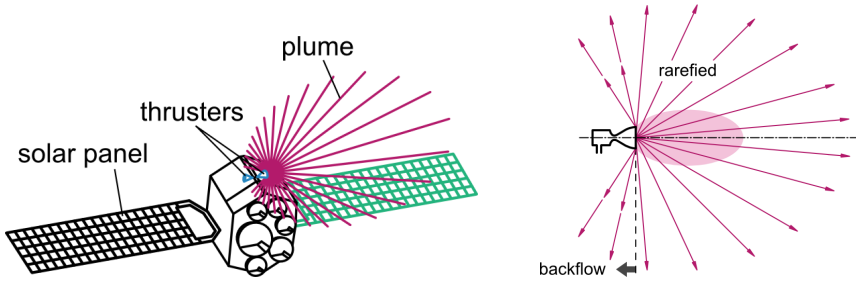

(a) Impingement of attitude control thruster plume

(b) Plume spreading in space

Figure 1

1 Introduction

Propulsion systems in space technology have to fulfil several requirements, among them high precision of thrust and impulse bit. The main cause in flight to fail the utility of this precision is plume impingement besides possible malfunction of the thruster itself.

Thrust in a propulsion device is produced by the directed ejection of propellant mass which is accelerated to preferably high velocity. It can therefore be quantified roughly by $F = \dot{m}u$, with mass flow $\dot{m}$ and velocity u. Once this mass has left the thruster and thereby produced the thrust F it is able to spread not only along the thrust axis, but also laterally and even backwards hitting the spacecraft (Fig. 1). Such impingement results in disturbing forces on the spacecraft and thereby depletes the precision of the propulsion system.

Plume impingement with its peculiarities is a faithful but undesired companion of all propulsion systems, single thruster as well as clustered, chemical as well as electric, large as well as small, small as well as tiny.

Besides disturbing forces, unwanted heat load, excessive contamination, erosion and electric interactions are possible impingement effects. All of them can lead to damage or malfunction. The specific problems depend on the spreading ability of the plume gas, on the accessibility of the plume to the spacecraft surfaces, on the exhaust gas characteristics (electrically neutral or charged), on its species and kinetic energy.

The assessment of thruster plume impingement on spacecraft surfaces is standard for each new spacecraft development program. The analysis comprises the assessment of secondary forces and torques as well as heating rates and potential contamination on sensitive spacecraft surfaces. Various types of engineering and scientific analysis software have been developed and are in use to support this assessment as well as experimental studies performed in the last fifty years.

Nevertheless plume flow and impingement remain ongoing issues in space technology. The reasons are manifold. New propulsion systems have been developed and have found access to application, among them the various types of electric propulsion. A new type of interaction with sputtering and electric interaction needs to be stud-

- Thruster type
- Thruster firing mode
- Thruster location on spacecraft
- Spacecraft and surfaces at risk
- Properties of surfaces (material, temperature)
- Plume description (numerical, model, experiment)
- Plume/Spacecraft interaction (continuum, rarefied)
- Impingement description for forces and heat transfer (numerical, model, experiment)
- Vacuum facilities (code validation, simulation of impingement situatuions, exploratory tests)
- Experience

Table 1: Aspects of plume- and plume impingement analysis

ied. New sizes have been found to be necessary for example microthrusters, where the term micro denotes the thrust regime in Newton. The miniaturization in some cases requires rectangular nozzle cross sections, which result in a guided expansion of the flow different from that in round nozzles. Clustering of thrusters to achieve certain thrust levels which cannot be provided by available single thrusters show new impingement phenomena not observed in single thruster devices. And finally, thrusters and impingement phenomena still exhibit a larger variety than is commonly expected.

Thrusters, plumes and plume impingement effects therefore continue to be studied to understand and predict their complete impact on the spacecraft. Experimental investigations are indispensable to validate and improve codes and to reveal actual thruster plume and impingement characteristics. On the other hand the application of validated numerical methods and tools can support the design and efficiency of experimental studies and improve the analysis of their results (a hand in hand development of experimental and theoretical work). And last not least some experience is necessary to detect potential problems and to assess them quantitatively.

A survey on plume flow and impingement in space technology has been given by one of the authors (G.D.) in 1991 [Dettleff, 1991]. In that article, emphasis was put on the depiction of chemical and cold gas plume model development and on force and heat transfer determination, whereas contamination and electric propulsion were omitted. In this article we will touch on the last twenty years with some numerical methods,

experimental facilities and results. We will concentrate on plumes and impingement effects related to small chemical and cold gas thrusters as they are used for operation of satellites and space probes. Some issues addressed in this paper are listed in Table 1.

To get somewhat familiar with the subject we describe some plume and impingement characteristics in the next section. After this rather qualitative depiction, we introduce in section 3 numerical tools and experimental facilities necessary to calculate and to measure plumes and impingement effects. In section 4 we present some aspects of plume analysis. We will show the value of exploratory experiments and the possible discovery of effects that were not predicted afore. Section 5 is devoted to examples of impingement situations and their investigation. Presented are also investigations on how to shield surfaces at risk.

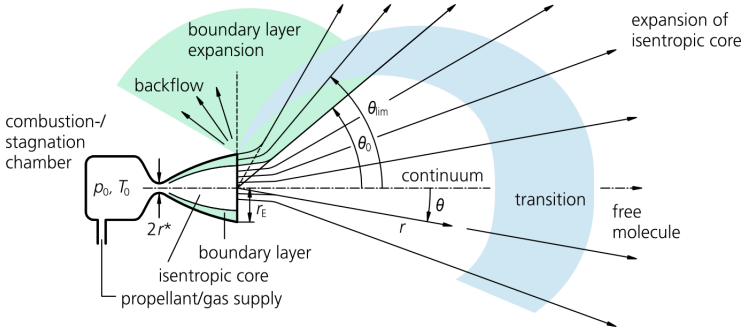

Figure 2: Thruster gas flow expanding into high vacuum: flow regimes

2 Plume and impingement characteristics

The plume and impingement characteristics depend primarily on the type of thruster. A great number of different chemical, cold gas and electrical types is in operation or under development. One of the most frequently used propellants for satellites and space probes is the bipropellant fuel/oxidizer combination CH_6N_2/N_2O_4[1]. Its advantage is a high specific impulse I_{sp} and the suitability for storage over several years of the mission. The combustion products are mainly N_2, H_2, H_2O, CO_2. In addition, a large number of chemical reaction products have been detected in minor concentration.

We take a thruster of this type to describe the most important features of plume flow with respect to impingement and follow the flow starting from the stagnation chamber (Fig. 2). Fuel and oxidizer are sprayed into the chamber and undergo a hypergolic reaction. The combustion products escape through the nozzle throat and the flow becomes supersonic, while initially chemical reactions continue. The guided expansion in the nozzle is characterized by the boundary layer along the wall and an isentropic core. In the isentropic core, the Mach number at the nozzle exit, where the freely expanding plume begins, is typically $Ma_E > 5$ (hypersonic flow).

In the plume we likewise distinguish between the expansion of the isentropic core ($\theta \leq \theta_0$ in Fig. 2) and of the boundary layer, as we did for the nozzle flow. Along the streamlines the density decreases to span from continuum flow in the vicinity of the thruster nozzle exit and rarefied flow far downstream and in the off-axis region, including the backflow.

Thinking of the plume as a purely expanding gas flow is not entirely correct. Firstly, due to the overexpansion behind the nozzle throat, and also due to the interaction of the supersonic flow with the nozzle wall, a compression shock system can be formed that reaches into the freely expanding plume. Such a compression influences the streamline pattern of the flow, i. e. it influences especially the density and velocity field (will be discussed in context of Figs. 16 and 17). Secondly the flow consists not only of gas, but also of unburned and polymerized fuel droplets, originally sprayed into the combustion chamber, i. e. we have to reckon with a two-phase flow.

[1] CH_6N_2 is known by the name mono-methyl hydrazine and frequently abbreviated MMH

Another possible source of liquid in the flow, besides unburned fuel, is the cooling film (not shown in Fig. 2) at the combustion chamber wall. Since the combustion temperature is about 3000 K, such cooling is necessary. When firing starts at cold condition (with nozzle temperatures of about $T_W = 300\,K$), this liquid film may be carried along the nozzle wall (driven by an interaction between the film and the boundary layer flow of the gas) towards the nozzle lip, where the liquid forms boiling droplets that burst and are thus ejected into all directions.

The interaction between the gas and the droplets begins in the flow out of the combustion chamber into the nozzle. Downstream of the throat the gas is accelerated to supersonic speeds (except in the immediate vicinity of the nozzle wall). The interaction can therefore be subsonic as well as supersonic, depending on the velocity lag, with a local compression in front of the droplet.

In the expanding flow the gas cools, and the interaction subsequently may lead to cooling of the droplets and heating of the surrounding gas. In addition, the droplets may evaporate (especially when the gas pressure falls below the vapour pressure of the droplets) and thereby contribute to the density and species composition of the plume gas. Another reason for a non-uniform plume gas composition is the mass separation effect due to the rapid expansion into the rarefied regime especially around the nozzle lip into the backflow region.

Lastly, we have to consider the development of the flow with time. Before firing, the temperature of the thruster is about $T_T = 300\,K$ and the pressure in the nozzle and combustion chamber is at ambient conditions, i. e. at the level of the vacuum surroundings. When the fuel and oxidizer valves are opened, the two liquids get in contact in the combustion chamber, ignition starts and the combustion products escape through the nozzle throat. A constant pressure in the chamber is attained when this mass flow through the throat is equal to the sum of the mass flows of fuel and oxidizer, which in turn is determined by the difference between the combustion pressure and the pressure in the storage tanks. While the thruster is in operation it experiences heating: The combustion chamber wall due to combustion, and the nozzle wall mainly due to interaction with the flow. The increase in temperature of the nozzle wall affects the boundary layer and thereby the plume. The temperature maximum is located at the nozzle throat. Lower temperatures are detected at the combustion chamber wall (due to the liquid cooling film) and towards the nozzle lip. A steady state temperature distribution is typically reached after about $t_{on} = 10\,s$ of continuous firing, when heat conduction in the walls and radiative heat loss from the walls have equilibrated. The qualitative description of this course of events suggests that the plume of a continuously fired chemical thruster takes about 10 s to reach steady-state as well. During the transient phase, the streamline pattern, the local gas density, velocity and plume gas composition may vary with time. Especially in the back flow variations are possible, since the boundary layer is the source of this rarefied flow.

During pulse mode firing a constant thruster wall temperature cannot be expected. Rather, a periodic temperature increase and decrease about local mean values characterizes steady state. Therefore, a single steady pulse within a pulse train actually is not possible. However, depending on the firing time and on the thruster wall temperature

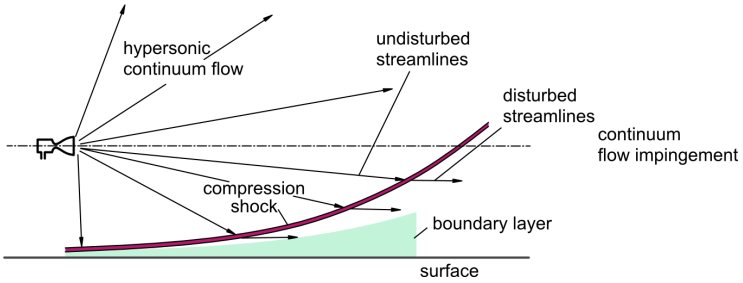

Figure 3: Continuum flow impingement on a technical surface

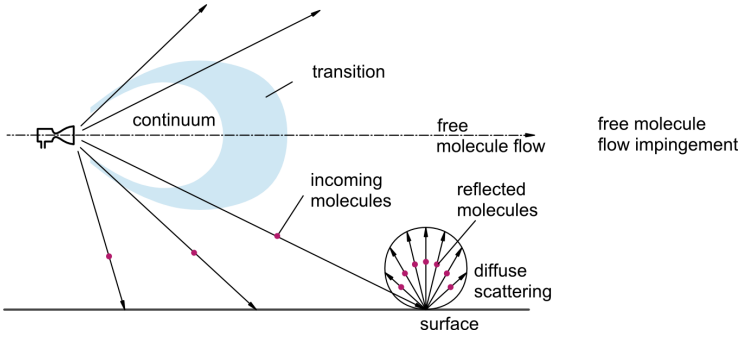

Figure 4: Free molecule flow impingement on a technical surface

and its variation, the plume may be considered as quasi-steady. In all three cases – continuous, pulse mode and single pulse firing – the steady state plumes (i. e. the ones at highest possible temperature level) will be different from plumes developed out of cold starting conditions.

When the thruster is shut off, i. e. fuel and oxidizer valves are closed, the combustion pressure, the mass flow through the nozzle and the gas density everywhere in the plume decrease, following roughly an exponential decay with time. The total duration of this process is several seconds, but it takes only a few milliseconds before the flow seizes to be dense enough to be regarded as a continuum.

We consider now the flow types in front of the impinged surface of the spacecraft. Magnitude and type of impingement depend on the size and shape of the surface and its location within the plume: In a continuum impingement scenario, a compression shock is formed in front of the impinged body and a boundary layer flow along the surface will form, Fig. 3. The flow properties inside this boundary layer determine the local force and heat load.

In the free molecule case (Fig. 4) the gas particles reach the surface undisturbed and are scattered, leaving the wall without interaction with the incoming gas. Consequently, the local plume flow properties at the location of the surface (together with the characteristics of the gas/surface-interaction) determine the impingement effects.

The impingement of droplets is of course also determined by the gas impingement type. Two forces govern the movement of the droplets: force of inertia and force

resulting from the interaction with the gas. If the first is dominating as in the free molecule case all droplets with a trajectory to the body will hit the surface. Otherwise as possibly in the continuum impingement case the droplets may be deflected by the disturbed flow in front of the surface.

The large number of parameters determining thruster operation, and therefore plume properties, and their mutual dependencies complicate a systematic investigation and suggest to temporarily simplify the problem for systematic investigation by omitting certain issues when investigating plume flow numerically and experimentally. Such simplification may involve the omission of chemical reactions, of unsteady processes and extremely high temperatures. Actually, so-called cold-gas thrusters with exactly these properties are applied in space technology. To study such a device therefore has one reason and one advantage: first, to predict plume and impingement effects on the spacecraft, where it is operating, and second, to study simplified models of chemical thrusters with a manageable number of parameters. The same holds for impingement effects. The development and application of numerical and experimental tools therefore concentrates on both chemical thrusters with mutually interdependent characteristics, and on cold-gas thrusters with a single gas species.

3 Numerical tools and experimental facilities

During the early days of plume impingement investigations, up to about 1980 to 1990, analytical model descriptions were the preferred tool to calculate plume impingement effects [Dettleff, 1991]. The necessary simplifications needed to establish a model and the mapping from chemical to cold-gas thrusters matched well. Since then, however, sophisticated numerical methods, namely Navier-Stokes and DSMC flow solvers, have been introduced and continuously refined. Nowadays, they are a common tool to determine plume flow and impingement quantities. Their vast application also in other fields of technology, for example aviation (Navier-Stokes) and rarefied flow in general (DSMC) leads one to expect further improvement, allowing to drop the once necessary simplifications step by step and to eventually allow numerical replication of the actual firing and impingement situation.

While the numerical tools have been improved remarkably during the last decades, the experimental facilities are in about the same condition as they were at the beginning of plume research about fifty years ago. One reason is simply that these facilities have done, and still do, a good job. Another reason is the considerable investment required to simulate space vacuum conditions during thruster firing in a ground facility.

3.1 Conventional vacuum chambers

We consider the capabilities and features of such facilities by example of the DLR contamination chamber in Göttingen/Germany. It is made of stainless steel. The shape is cylindrical, with a height of more than 2.5 m and a diameter of about 2.2 m (Fig. 5). It is equipped with six big flanges with a diameter of 50 cm and numerous smaller flanges for vacuum feed-through. The six flanges can be used for various purposes, for example one is reserved for the thruster test rig (thruster and propellant supply), two of them can be equipped simultaneously with windows for optical observations and another one can be used for the installation of a turbomolecular pump.

The pumping system consists of two lines, each equipped with three pumps in series (Heraeus E225, RA2000 and RA7000 and Heraeus E100, RA2000 and RA7000). The roots blowers (RA) have nominal pumping speeds of 2000 m^3/h and 7000 m^3/h. The effective pumping speed has been determined experimentally by pouring Nitrogen into the evacuated chamber at constant mass flow. The background pressure p_b has been determined as a function of the mass flow. The effective pumping speed has been found to be about 12000 m^3/h.

The background gas pressure is given as

$$p_b = \frac{\dot{m}_p R_b T_b}{S(p_b)}, \tag{1}$$

where $\dot{m}_p$ is the pumped mass flow, R is the specific gas constant, T_b is the temperature of the background gas and $S(p_b)$ ist the pumping speed, which is a function of the background pressure.

Figure 5: The DLR contamination chamber (CCG) in Göttingen/Germany

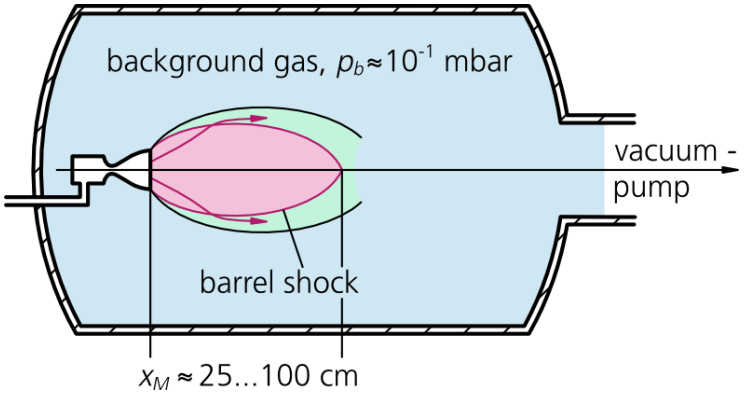

Figure 6: Limited plume expansion in a conventional vacuum chamber with barrel shock

The background pressure before thruster firing is typically $p_\mathrm{b} < 10^{-3}$ mbar.[2] Because of the limited pumping capacity, p_b increases when a certain mass flow $\dot{m}_\mathrm{T}$ is discharged by a thruster. When $\dot{m}_\mathrm{p} = \dot{m}_\mathrm{T}$, p_b reaches a constant value in Eq. (1).

Example. A 10N bipropellant thruster ejects about 3.5 g/s. With $S = 12000\,\mathrm{m^3/h}$, $R_\mathrm{b} = 400\,\mathrm{J/kgK}$ and $T_\mathrm{b} = 300\,\mathrm{K}$ we obtain a steady-state background pressure $p_\mathrm{b} = 126\,\mathrm{Pa} = 1.26\,\mathrm{mbar}$.

A plume in such vacuum chamber surroundings can only perform a limited expansion. The background gas acts as a barrier for the expanding hypersonic plume flow, which results in the establishment of a compression shock system (barrel shock, Fig. 6). Upstream of the barrel shock, however, the supersonic plume is unaffected by the background gas. Within this limited region, we can observe the flow just as if it were in an undisturbed plume in space vacuum. Whenever the downstream near-field of the plume has to be investigated, such a conventional vacuum chamber is therefore sufficient for many experiments.

The size of the confined plume (Fig. 6) may roughly be computed as proposed by [Ashkenas and Sherman, 1966] for free-jets from sonic orifices:

$$x_\mathrm{M} = \frac{2}{3} d^* \sqrt{\frac{p_0}{p_\mathrm{b}}}, \tag{2}$$

with nozzle throat diameter d^* and stagnation pressure p_0, or according to Driftmyer [Driftmyer, 1972] as:

$$x_\mathrm{M} = \frac{d_\mathrm{E}}{2} \sqrt{\kappa \frac{p_\mathrm{E}}{p_\mathrm{b}}} \mathrm{Ma_E}, \tag{3}$$

with nozzle exit diameter, pressure and Mach number $d_\mathrm{E}, p_\mathrm{E}, \mathrm{Ma_E}$, respectively, and the ratio of specific heats, κ.

[2] In vacuum technology it is customary to give pressures in millibar (mbar) instead of Pascal (Pa)

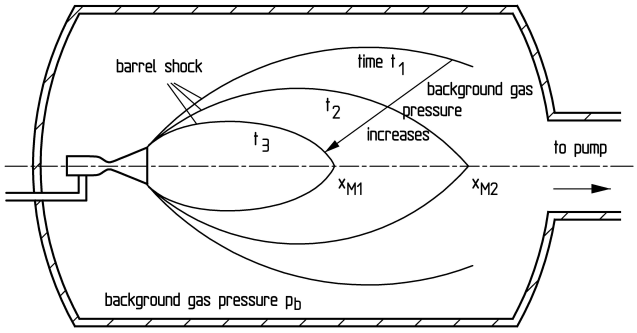

Figure 7: Development of barrel shock system after ignition of the thruster, $x_M \propto 1/\sqrt{p_b(t)}$, $t_1 < t_2 < t_3$. Steady-state when $p_b = \text{const.}$ and $\dot{m}_T = \dot{m}_p$.

The maximum diameter of the barrel is roughly

$$d_M = \frac{x_M}{2}. \tag{4}$$

As can be seen from equations (1), (2) and (4), the pumping speed determines the background pressure p_b and thereby the plume size.

The size and location of the shock system change with time after ignition. Indicated in Fig. 7 is the shrinking shock size at times $t_1 < t_2 < t_3$, where t is in the order of milliseconds. Consequently, the undisturbed flow region becomes smaller. Steady state size during continuous firing is reached after a few milliseconds when the mass flow exhausting from the thruster is equal to the mass flow pumped. Then the barrel shock size, characterized by x_M and d_M, reaches its minimum at steady-state.

Example. With the help of Eq. (2) and assuming that p_b is a linear function of time, one can estimate when the computed value of the axial plume extent will be $x_M < 2\,\text{m}$, i. e. smaller than the diameter of the vacuum chamber. Such consideration is necessary when a wide body shall be impinged. For a 10N bipropellant thruster with $\dot{m}_T = 3.5\,\text{g/s}$, $p_0 = 10\,\text{bar}$ and $d^* = 3\,\text{mm}$ we find $x_M = 2\,\text{m}$ after about 20 ms. Only during this time an undisturbed plume flow would impinge on a wide body and only during this short time the simulation of this scenario would be correct.

The situation in space is different, however. When the thruster is shut off in the vacuum chamber, the combustion breaks down. The combustion pressure p_0 decreases much faster than the background gas pressure p_b. As a consequence, according to (2) and again assuming for the moment that the pressures may be treated as time-dependent, the plume size shrinks and unlike in space the barrel shock system in the vacuum chamber moves upstream (i. e. towards the nozzle), potentially passing probes or impinged surfaces. The pressure of the background gas instantaneously after shut off is typically in the order of $10^{-2} \ldots 1\,\text{mbar}$. This means that the (rarefied) gas flow still emanating from the thruster for several seconds is destroyed. Therefore, all observations of the gas flow following the breakdown of the barrel shock system must be considered with particular care, since the situation is different in space.

Similarly, when operating the thruster in pulse mode, unburnt fuel and oxidizer escape during the first few milliseconds between opening of the valve and ignition and expand through the nozzle as a rarefied flow which is difficult to detect in a vacuum chamber at $p_b > 10^{-3}$ mbar. Though the amount escaping per valve opening is small, it is evident that the accumulated propellants in space, even if they evaporate with time, can harm neighboured surfaces after impingement.

During pulse mode firing, a steady-state background gas pressure is practically not possible. After some pulses, the pressure varies periodically between a maximum (at thruster shut-off) and a minimum value (immediately before thruster valve opening). A characteristic mean pressure is obtained when $\dot{m}_p$ in (1) is substituted by

$$\dot{m}_f = \dot{m}_T \left(\frac{t_{on}}{t_{on} + t_{off}} \right), \tag{5}$$

where $\dot{m}_f$ is the actual mass flow during firing time.

Example. Compare the resultant background pressure of the steady-state thruster operation in the example on page 11 with the pressure attained with a pulsed thruster. If we choose for example $t_{on} = 100$ ms, $t_{off} = 400$ ms we reduce the resulting background pressure to $p_b \approx 0.25$ mbar.

We have seen that the plume flow in the vacuum chamber is mainly affected by the background gas. If the droplets need to be considered, the force of gravity must be taken into account and also the interaction between the droplets and the plume gas.

Besides the test rig with its thruster-specific configuration the facility is equipped with traversing devices for probes. Measurement devices for background gas pressure and temperature are as well basic equipment for such a facility.

3.2 The need for a high-vacuum plume test facility

Facilities like the CCG have been and are still used for many investigations. Careful attention to the restrictions allowed many successful measurements in the continuum plume nearfield. The listed deficiencies, however, and the missing access to the rarefied regimes, especially the backflow region, triggered the idea of a ground facility in which space vacuum conditions can be achieved. DLR built and operates its unique high-vacuum plume test facility STG (in German: Simulationsanlage für Treibstrahlen in Göttingen), in which plumes of small thrusters can spread into a vacuum of $p_b < 10^{-5}$ mbar. Under such conditions also the highly rarefied regime, including the backflow is reproduced.

The essential feature of the facility STG is a liquid-helium-driven cryopump with an area of about 30 m^2 (Fig. 8). The cylindrical cold surface completely encloses the plume expansion section. Since hydrogen is an essential exhaust constituent, it is necessary to cool the cryopump to at least 4.7 K. At this temperature, the vapor pressure of the condensed H_2 is $< 10^{-5}$ mbar, which is considered the highest pressure at which plume spreading and plume impingement is reproduced in space-like conditions. Effectively, the temperature on the cryopump surface is about 4.3 K before thruster firing.

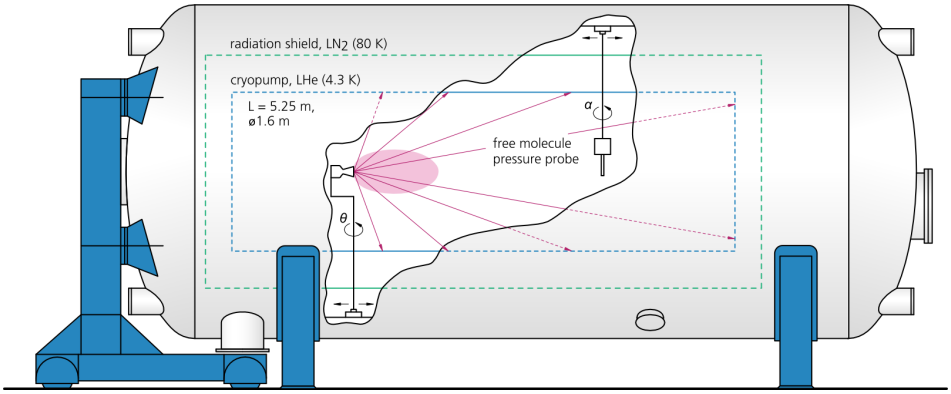

Figure 8: The DLR high-vacuum plume test facility (STG) in Göttingen/Germany. Main features and test set-up.

If no hydrogen is present, for example in tests with cold-gas thrusters or so-called "simulated plumes" with inert plume test gases, the pressure in the test section is less than 10^{-7} mbar.

The cylindrical cryopump (length 5.25 m, diameter 1.6 m) is enclosed by a likewise cylindrical radiation shield which is cooled with liquid nitrogen to about 80 K to protect it from the heat radiated off of the steel chamber walls. Both cold walls are installed in the stainless steel vacuum chamber that has a total length of 7.6 m and a diameter of 3.3 m. Two longitudinal slots are provided at top and bottom to allow for feed through of mounting devices for the probes and thruster. The traversing devices are mounted to the stainless steel vacuum chamber wall to maintain them at about room temperature and thus to avoid failure due to cold-contraction. A second cooling system for pre-cooling with liquid nitrogen is integrated into the cryopump, separated from the LHe-circuit. In addition, the chamber is equipped with mechanical pumps in addition to the cryopump. First, there are a rotary vane and two roots blower pumps connected in series with a combined pumping speed of about 3000 m^3/h. This set of pumps is required for initial evacuation to about 10^{-3} mbar, before the cooling with liquid nitrogen begins and also to evacuate the condensed gases after the test run. Then also the turbomolecular pumps (pumping speed 1.5 m^3/s) are put into operation (with the roots pumps as fore-pump; the gate valve between this set of pumps and the chamber is now closed). The main purpose of the turbomolecular pumps is to evacuate helium which may escape from the cryopump system, since tiny leaks in the order of 10^{-7} mbar · l/s are possible at the connecting flanges (helium cannot be pumped by the cryopump). Thus the possible partial pressure of gaseous helium (GHe) in the chamber can be kept below 10^{-7} mbar and does not impair the free plume gas expansion. Another purpose of the turbomolecular pumps is to allow the long-lasting degassing procedures of the equipment before the experiment, without expensive cryopumping.

A flow chart of the whole facility STG is shown in Fig. 9. To cool the radiation shield and the cryopump down to 80 K, liquid nitrogen is taken out of the tank. Further

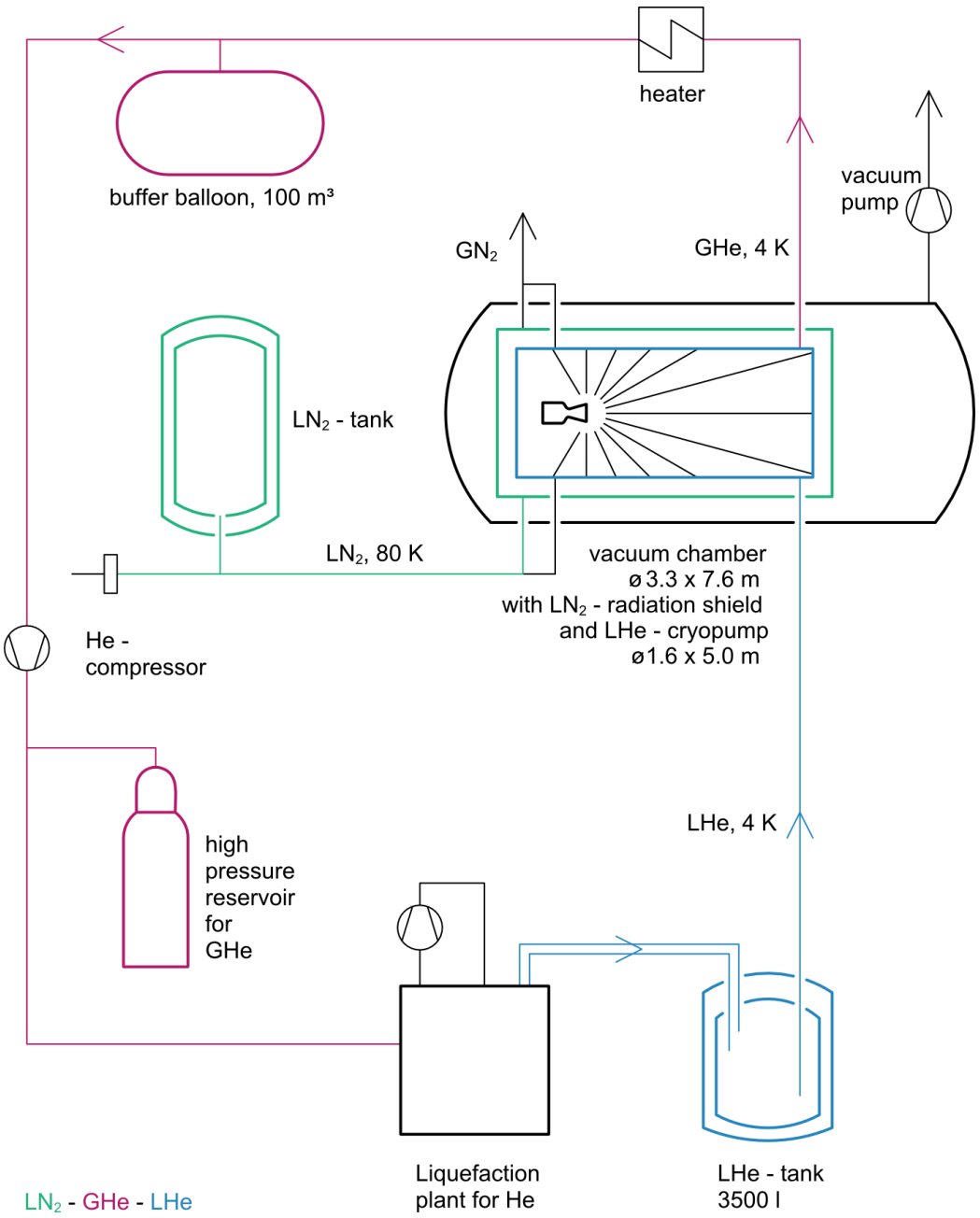

Figure 9: Flow chart of the DLR high-vacuum plume test facility STG

cooling of the cryopump is performed by liquid helium taken out of the tank with a volume of 3000 l. The liquid helium in the tank is kept at about 1.3 bar and is transferred to the cryopump (1.0 bar) purely by the pressure difference. About 1000 l of LHe are required to cool the cryogenic pump and to fill it. Inside the cryopump the helium is in the boiling state at $T = 4.2$ K. The impact of the plume gas and its freezing on the cold surface cause a heat transfer into the cold wall to the boiling helium, which hence evaporates. The evaporated helium is transferred via a heater, a buffer balloon of 100 m^3 and a compressor (175 m^3/h) to a high-pressure reservoir. The gaseous helium is liquefied again with a rate of about 20 l/h.

The design of the cryopump was guided by the demand to simulate steady plumes with a total heat load of about 500 W. For plumes from small chemical thrusters (thrust level up to about 1 N) all flow types, including the highly rarefied backflow, can be realized in steady-state. Thus the principal intention to validate codes and to simulate impingement situations in all flow regimes is reflected.

The usability of the facility is however not limited to these applications. Larger thrusters can be operated in STG as well, if they are fired in pulse mode, especially with single pulses. After ignition, the cryopump temperature increases rapidly. Firing must be terminated before the cryopump temperature reaches 4.7 K. For a 10N bipropellant thruster this restriction results in firing times of about 400 ms, sufficient to perform measurements. But it is also possible to exceed the temperature of 4.7 K locally and to extend the test time. Obviously, the gas would be trapped for a while in a layer in front of the cryopump, before it is detected as disturbing background gas at the location of measurement.

3.3 Numerical Methods

Gas expanding from a nozzle into vacuum exhibits a wide range of density and flow velocity, which makes efficient numerical flow simulation a non-trivial task. From a physical point of view, methods of rarefied CFD, which recognize the particulate nature of gas, may be applied to compute the flowfield of the entire expansion, both guided (nozzle) and free (plume). As these methods resolve scales on the order of a mean free path, they tend to be expensive in denser flow domains, particularly inside the nozzle. As such a fine resolution is not required here, a macroscopic perspective may be assumed and the flow may be treated as a continuum. Methods of continuum CFD have achieved a high level of maturity and are typically a lot faster in their range of applicability. In order to use these two approaches concurrently however, one needs to establish criteria for where continuum CFD can be expected to yield physically correct results.

3.3.1 Rarefied CFD

It is customary to characterize the degree of rarefaction by a dimensionless parameter known as the Knudsen number. It relates the mean free path of the particles in the gas to a geometric length that is characteristic for the problem under investigation. Even

though local Knudsen numbers may be very low, especially in the convergent part of the nozzle, the gas may be considered rarefied in the sense that molecular interaction may be regarded as instantaneous and predominantly involving two molecules. From a physical point of view, numerical methods based on these prerequisites are applicable to the study of gas flow in the nozzle and subsequent plume expansion.

The numerical methods developed for the simulation of rarefied flows may be grouped into two categories according to their general approach: One is the deterministic approach, that aims at solving the Boltzmann equation or a similar model equation with the various tools available to numerical mathematics. The other approach to compute rarefied flow-fields is to use probabilistic methods that compute the motion and interaction of particles with each other and with the boundaries of the computational domain.

Arguably, the method most widely used in engineering applications is termed Direct Simulation Monte-Carlo (DSMC). It may intuitively be described as an experiment carried out in the computer, using a large number of simulator particles to represent the seemingly uncomputable number of real molecules that make up the gas flow in typical engineering problems. These simulator molecules move and probabilistically collide with neighboring simulators in decoupled cycles. Macroscopic flow parameters, such as density, velocity and temperature(s) are determined from averaging over many time-steps. A thorough description of DSMC is given in Bird's 1994 monograph [Bird, 1994], though the algorithm has been significantly advanced since then [Bird et al., 2009, Gallis et al., 2009].

3.3.2 Continuum CFD and Code coupling

While it is desirable and physically possible to compute the flow both, downstream of and inside the nozzle with the methods of "rarefied CFD", the computational requirements of these methods typically increase with increased density. For an introduction to continuum CFD, see e.g. the book of Anderson [Anderson, 1995].

The idea to save on computational resources by using dedicated continuum flow solvers where applicable, and interface them to a solver for rarefied flows appeals to many researchers. The combination of Navier-Stokes solvers with DSMC seems to be the most popular, as mature implementations of both are fairly available. Hybrid computations relevant to plume expansion and impingement have been carried out e. g. by Lumpkin et al. [Lumpkin et al., 1995, Lumpkin et al., 1996], Gatsonis et al. [Gatsonis et al., 1999], and more recently by Papp et al. [Papp et al., 2006]. For an overview on coupling, see also the lecture notes of Boyd in this series.

It is possible to combine the two codes in three ways, distinguished by the directions and the frequency, in which information is exchanged. The most simple approach is to run both codes entirely separated from another. Usually, the entire flow-field is first computed with a Navier-Stokes solver. From this initial solution, the validity limit of the continuum assumption is determined by a suitably chosen continuum breakdown parameter. Along the validity limit the continuum flow-field is cropped and the inflow boundary conditions for the DSMC simulation are extracted. The latter is than

run independently. The fidelity of this kind of simulation is best, when the flow speed component perpendicular to the coupling interface is supersonic, preferably hypersonic. A more refined variant of this approach would be to regularly update the the Navier-Stokes ouflow boundary as well. Lastly, a tight, time accurate up-/and downstream coupling of the two solvers would be the most complete, but also most difficult approach. Much of the difficulty arises from the statistical scatter inherent in DSMC solutions that would adversely affect the stability of the Navier-Stokes solver.

3.3.3 Continuum breakdown parameters

Several indicators signalling inapplicability of continuum assumption and thermal equilibrium have been described in the literature and new suggestions are occasionally published. We restrict ourselves here to a short review of the most frequently used approaches to determine continuum *breakdown*, i. e. to parameters that are conveniently computed from the solutions of a Navier-Stokes solver.

A popular parameter indicating thermal non-equilibrium in expanding, isentropic, hypersonic flows has been suggested by Bird in 1970 [Bird, 1970]. It relates the logarithmic lagrangian time-derivative of the density ρ in a fluid element to the collision frequency ν in that element:

$$P = \frac{1}{\nu}\left|\frac{\mathrm{D}(\ln\rho)}{\mathrm{D}t}\right|. \tag{6}$$

The expression simplifies in case of steady, one-dimensional flow to

$$P_1 = \frac{1}{\nu}\left|\frac{u}{\rho}\frac{\mathrm{d}\rho}{\mathrm{d}x}\right|. \tag{7}$$

Other researchers prefer to use Knudsen numbers based on local gradient lengths [Smolderen, 1965, Bird, 1994]: Boyd

$$\mathrm{Kn}_Q = \lambda\frac{|\nabla Q|}{Q}, \quad Q \in \{\rho, u, T\}. \tag{8}$$

where usually the maximum Kn_Q for any flow-field parameter Q is chosen, see e. g. Wang and Boyd [Wang and Boyd, 2002].

3.3.4 Required solver capabilities

The numerical treatment of nozzle flow and plume expansion for engineering problems requires a set of solvers with various fidelity and boundary conditions. The part of the flow that may be regarded as a continuum certainly requires at least a compressible Navier-Stokes-Fourier solver, as flow speeds are high (mostly supersonic) and viscosity and heat conduction are important to model.

The presence of rather thick boundary layers in the nozzle, especially for cold-gas thrusters, may be an incentive to include slip wall boundary conditions. When computing only the flow inside the nozzle, using an exit-pressure boundary condition at

the nozzle exit is advisable from a numerical point of view, as subsonic regions of the boundary layer must be taken into account.

When using continuum CFD results as inflow boundary conditions to a DSMC solver, the interface must be chosen such that the constraints of physical validity are fulfilled for the continuum CFD code, and that the flow speed normal to the coupling interface is supersonic. In this case, both computations may be carried out in a detached manner. For consistency, the particles generated at the inflow boundaries in the DSMC method should follow a Chapman-Enskog velocity distribution. When simulating free plume expansion in space, the DSMC outflow boundary condition is much simpler: A perfect vacuum is simulated by simply deleting particles that leave the flowfield and not generating new ones.

4 Plume analysis

It has been mentioned in the previous section that suitable numerical methods allow for the computation of entire flowfields around actual engineering configurations. To do so, however, a detailed knowledge of the employed thruster and its firing mode is indispensible. The propellants used, the combustion temperature and pressure, the composition of exhaust products and lastly the shape and state of the nozzle wall, all affect the plume's mass, momentum and energy distribution. Once characteristic plume parameters (namely density and velocity) are known, one can proceed to estimate forces and heat loads due to impingement onto surfaces potentially at risk.

A systematic analysis of plume impingement effects demands a thorough understanding of the undisturbed plume itself. In this section we touch on some aspects of plume analysis, focussing on experimental techniques to characterize the plumes of chemical and cold-gas thrusters.

4.1 Contamination potential

As contamination is a major concern with the application of chemical thrusters in space we will devote special attention to it and define *contamination potential* by all gaseous and liquid constituents in the plume which are able to stick to a surface for an unallowable time. Whether a surface is considered contaminated after it has been impinged by a thruster plume thus also depends on the surface properties itself. A cryogenically cooled surface for example is contaminated when hit by gas components which could freeze at wall temperature. On other surfaces the same gas may be harmless.

In chemical thrusters a special contamination threat is due to droplets of (partially) unburnt fuel or from residuals of the cooling film that mitigates the heat load onto the combustion chamber wall in some thruster types. Also, there will be fuel droplets originating from the combustion chamber during the short transient phase between opening the thruster valve and ignition.

Including the treatment of the liquid phase within the plume analysis is somewhat more complex as it also comprises the interaction between the droplets and the gas flow. Experimentally, droplets and hence their contamination potential can be detected directly in the flow or on witness plates. Of interest are especially those droplets that do not evaporate immediately after firing and deposition.

In order to detect the presence of harmful droplets in the immediate rearward vicinity of the thruster, a nozzle collar acts as a simple witness device to simulate an adjacent spacecraft surface. Figure 10 illustrates size and location of a collar.

In the course of an experiment with a 10 N bipropellant thruster, non-evaporating droplets have been collected on the collar and remain there, both in vacuum and in under ambient conditions (Fig. 11). By non-evaporating we mean in this context that no weight loss can be detected within 24 hours. The contamination must accordingly be assumed to be permanent. The presence of these backflow droplets was a previously not predicted finding for us that emerged from exploratory tests with bipropellant thrusters. Note that not the impingement itself is the object of study here, but its effect

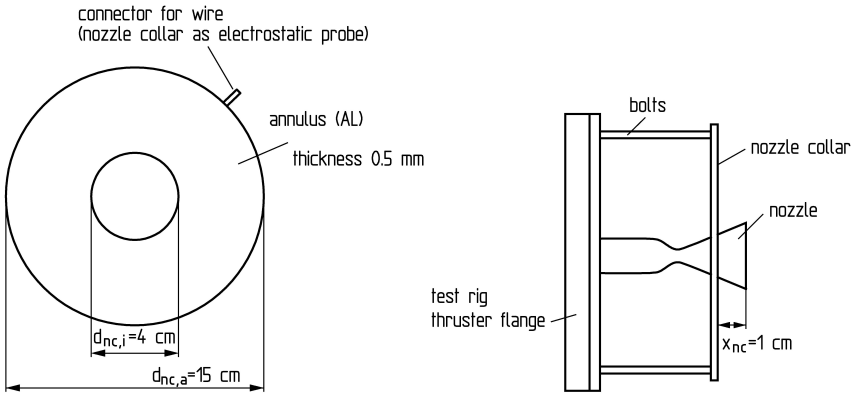

(a) Nozzle collar (annulus) (b) Mounting of the nozzle collar

Figure 10: Nozzle collar to detect contamination potential

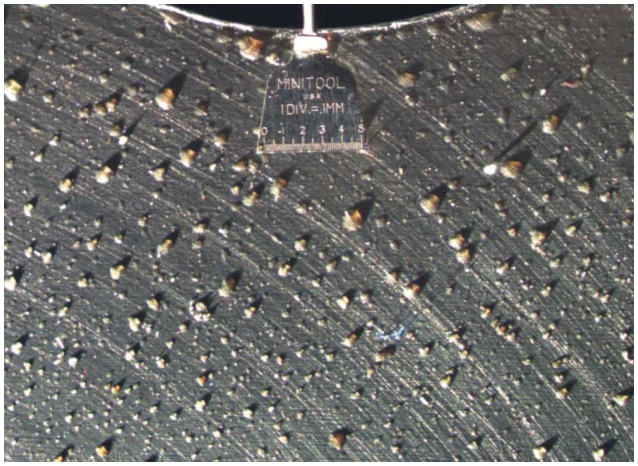

Figure 11: Persistent droplets of incompletely burnt fuel on nozzle collar (bipropellant thruster)

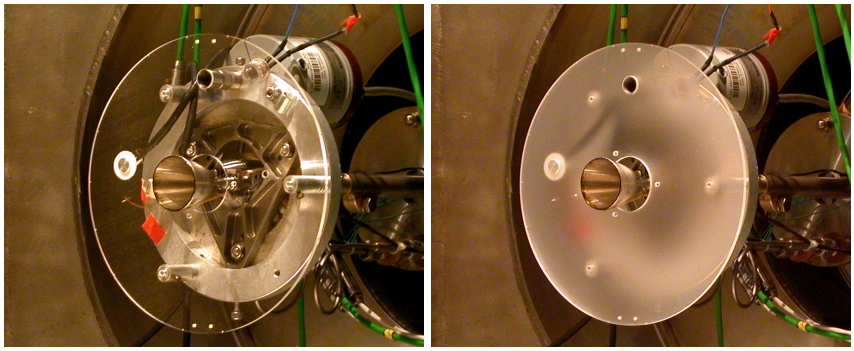

(a) clean collar (before firing) (b) contaminated collar (after firing)

Figure 12: Bipropellant thruster with acrylic glass collar

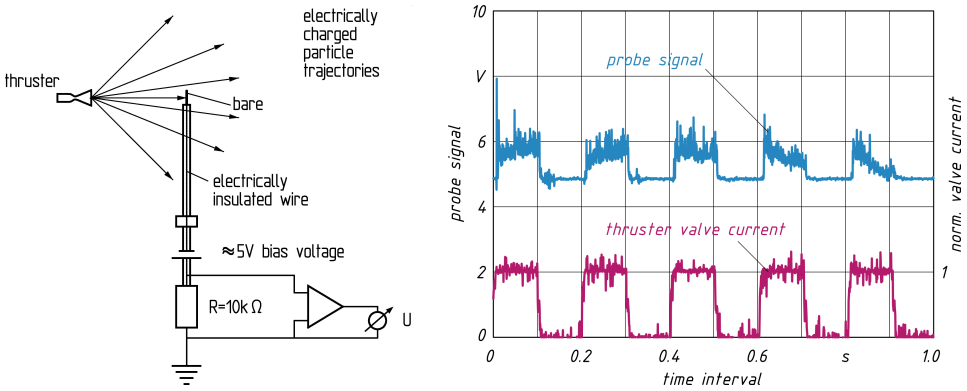

(a) Basic setup (b) Typical signal in pulse-train

Figure 13: Electrostatic (wire) probe. A bias of 5 V is applied to the probe signal.

is used to characterize a plume property.

Depending on the thruster and the firing mode (e. g. the on/off times in a pulse train) the distribution and size of the deposited contaminants lead to quite different coatings of the collar, indicating a different contamination potential. While the contaminated collar shown in Fig. 11 clearly shows distinct droplets, a milky film was observed in other experiments employing acrylic glass collars, Fig. 12. In the latter case the acrylic glass permits to measure and compare optical transmittance of the clean and the afterwards contaminated device. This is especially important when the impact of contamination on optical surfaces must be quantified. One then conducts the optical transmittance measurement with light of the relevant wavelengths.

There are several methods for time-resolved droplet detection without hindering the plume expansion. A conceptionally simple device is the electrostatic pressure probe, a sketch of which is shown in Fig. 13a. The electrode (i. e. the bare end of the wire) may be probed at various locations in the plume and if electrically charged droplets hit the wire they produce a voltage signal, see Fig. 13b for exemplary experimental data. In

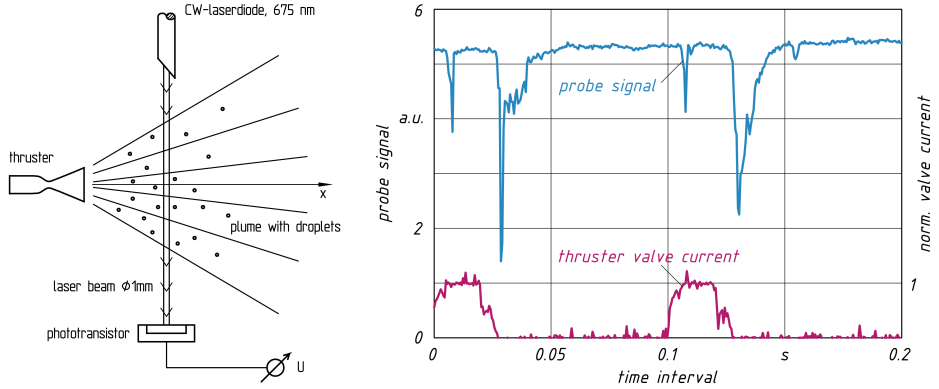

(a) Basic setup

(b) Typical signal in pulse-train

Figure 14: Laser beam attenuation

this way a qualitative picture of the droplet distribution (i. e. contamination potential) in both time and space is found. If no electrically charged droplets were present, the signal would simply be a straight line at 5 V (bias).

Another method to detect the presence of droplets exploits the attenuation effect a droplet-laden plume has on a laser beam (Fig. 14a). This technique is unintrusive, but only resolves integral line-of-sight rather than individual points in the flow field. Qualitatively, however, one may obtain time-resolved information on the droplet density during thruster firing cycles. Figure 14b for example shows the change of recorded laser light intensity during and after two 20 ms pulses from a bipropellant thruster. The small signal dip lagging after thruster valve opening is possibly caused by liquid propellant components from right after injection, before combustion commences. The more pronounced signal drop arises from unburnt fuel left in the combustion chamber after the valve has been shut and combustion breaks down. Note, however, that the signal dip is detected notably after the thruster valve closes. As these results were obtained in a conventional vacuum chamber (CCG), they must be interpreted with particular care, see Sec. 3.1.

The experiments described in this section are of an exploratory nature and serve to indicate contamination potential of a thruster. Whenever more detailed information is required, the experiments of cause need to be more detailed as well.

4.2 Pitot pressure measurement

A very simple device to explore the structure of the gas flow in the nozzle and in the plume near field is the Pitot probe. It measures the pressure of a fluid brought to rest. Figure 15 shows two probe configurations that may be used for plume analysis, they essentially differ in the the range of pressures to which they may be applied. Note that as the gas flow in and downstream of the nozzles under consideration here is supersonic everywhere (except in parts of the boundary layer), a shock will form in front of the probe and the signal measured will be the total pressure behind the shock,

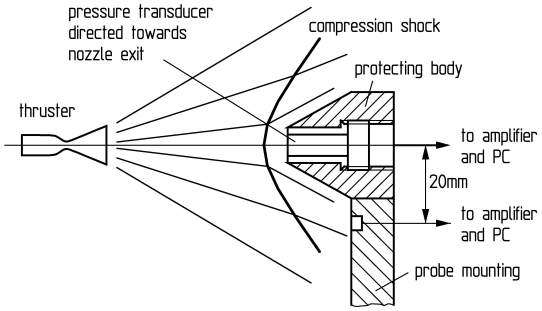

(a) Kulite pressure transducer

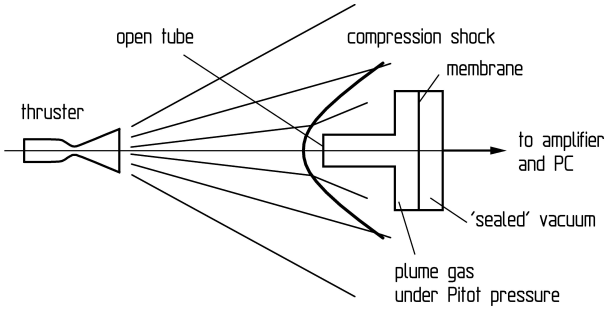

(b) MKS Baratron pressure transducer

Figure 15: Experimental setup for Pitot pressure measurement

p_{t2}, which is generally lower than the total pressure of the undisturbed flow.

The plume region ultimately downstream of the nozzle exit may be regarded as a continuum hypersonic flow, and it is well known that in this case the measured Pitot pressure may be related to density ρ and flow speed u of the undisturbed stream as:

$$p_{t2} = \frac{\kappa + 3}{\kappa + 1} \frac{\rho u^2}{2}. \tag{9}$$

Hence, if the ratio of specific heats, κ, and u can be estimated (for example in the far field from the chemical reactions and the composition of the gas) Pitot pressure profiles reflect directly the density distribution in the plume. The result is of course only a rough density pattern but maybe sufficient to solve a particular local problem.

The plume density varies roughly with the inverse square of the distance from the nozzle, and consequently the gas flow quickly gets more and more rarefied. The Pitot probe will then still deliver a signal, but the interpretation changes. While in continuum, $p_{t2} \propto \rho u^2$ (indicating a net momentum flux, i. e. pressure) the signal tends towards being proportional to the mass flux ρu as the flow becomes more and more rarefied and intermolecular collisions cease to dominate the transport of energy and momentum. In the free-molecule, i. e. collisionless limit, the probe behaves similar to the so-called Patterson probe treated in the Sec. 4.3. Regardless of the degree of rarefaction however we always have a probe signal directly proportional to density. The factor of proportionality however varies with the rarefaction.

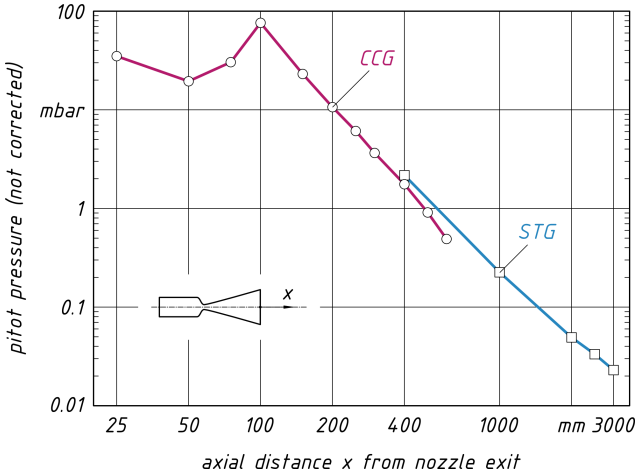

Figure 16: Pitot pressure signals measured along the plume axis of a bipropellant thruster

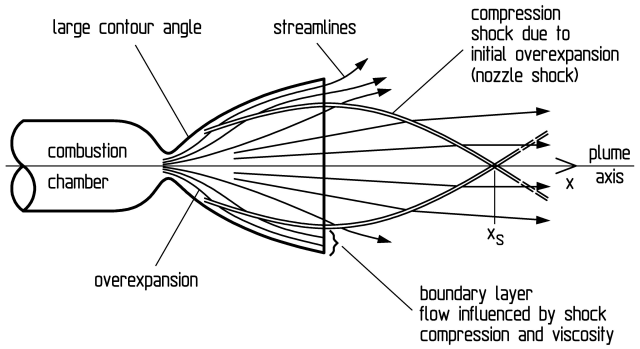

Figure 17: Flow pattern in and downstream of a contoured nozzle (schematic)

An example of how the raw Pitot probe signal varies with increasing axial distance from the exit plane of a contoured nozzle is given in Fig. 16. The data is presented here directly as measured, i. e. no corrections have been applied to account for rarefaction effects. Measurements are made for the same thruster in different facilities. Near field data was obtained from experiments in the conventional vacuum chamber CCG (Fig. 5 on page 10), while far field results were recorded for the freely expanding plume in STG, see Sec. 3.2.

It is worthwhile to remark on the peak of probe signal at around 100 mm downstream of the nozzle exit plane. This peculiarity of contoured nozzles becomes clear when looking at Fig. 17: The rapid change in curvature just after the nozzle throat leads to an overexpanding supersonic flow that subsequently is forced back to be parallel to the nozzle wall. This change of direction causes compression shocks that manifest themselves in the Pitot measurements.

To give an impression of the range of flow regimes in terms of rarefaction in this

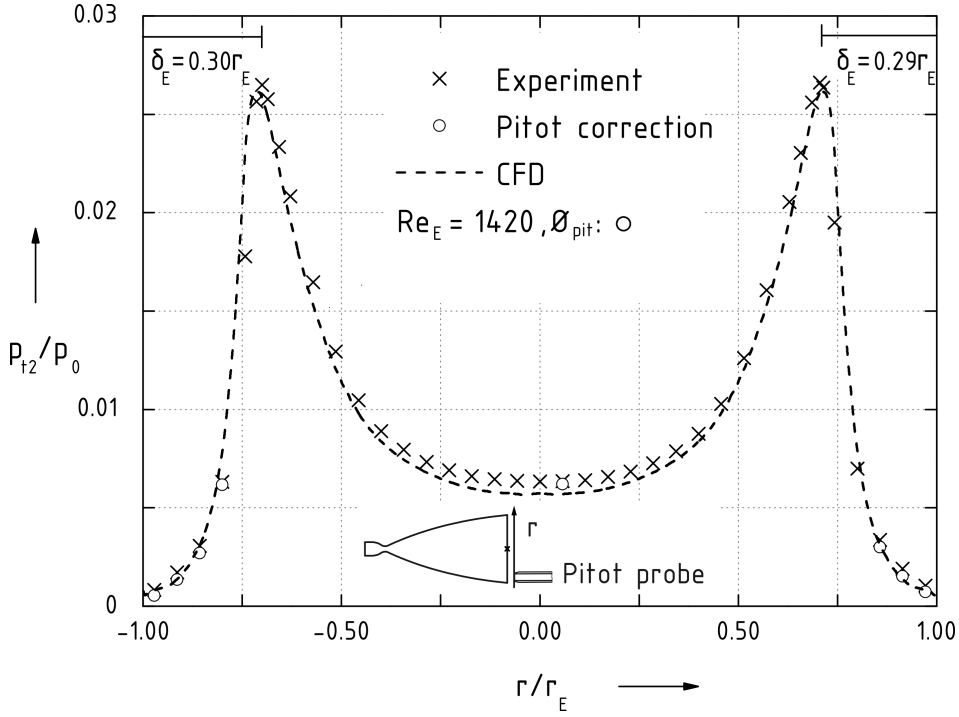

Figure 18: Calculated and measured pitot pressure profiles (adapted from [Traphan, 2011])

profile, it is instructive to give an estimate of the probe Knudsen number near and far away of the nozzle exit. At an axial distance of $x = 3\,\mathrm{m}$ the gas mean free path is in the order of about $\lambda \approx 1\,\mathrm{m}$, while closer to the nozzle ($x = 0.2\,\mathrm{m}$) we have $\lambda \approx 1\,\mathrm{mm}$. For a probe of diameter 10 mm, this leads to Knudsen numbers of $\mathrm{Kn}_{x=3\,\mathrm{m}} \approx 100$ (highly rarefied) and $\mathrm{Kn}_{x=0.2\,\mathrm{m}} \approx 0.1$ (weakly rarefied), respectively. Exact values of course depend on the stagnation conditions of the investigated thruster but the orders of magnitude are representative.

Figure 18 shows a Pitot pressure profile measured across the exit of a cold-gas thruster with contoured nozzle. The Pitot pressure profile computed with continuum CFD (here using the DLR TAU code) for the same condition is also plotted for comparison. The relatively good agreement leads one to expect that other flow properties that were not measured directly (such as density, velocity and temperature) can be reliably computed.

One such radial section of computed values in the nozzle exit plane is depicted in Figure 19. The black curve represents the Pitot pressure profile, and the red, green and blue graphs show speed, temperature and density, respectively. The combination of experiment and numerics yields information about the flow that was otherwise hardly accessible in the experiment. Likewise, confidence in the numerical methods can only be gained from comparison with reliable experimental data.

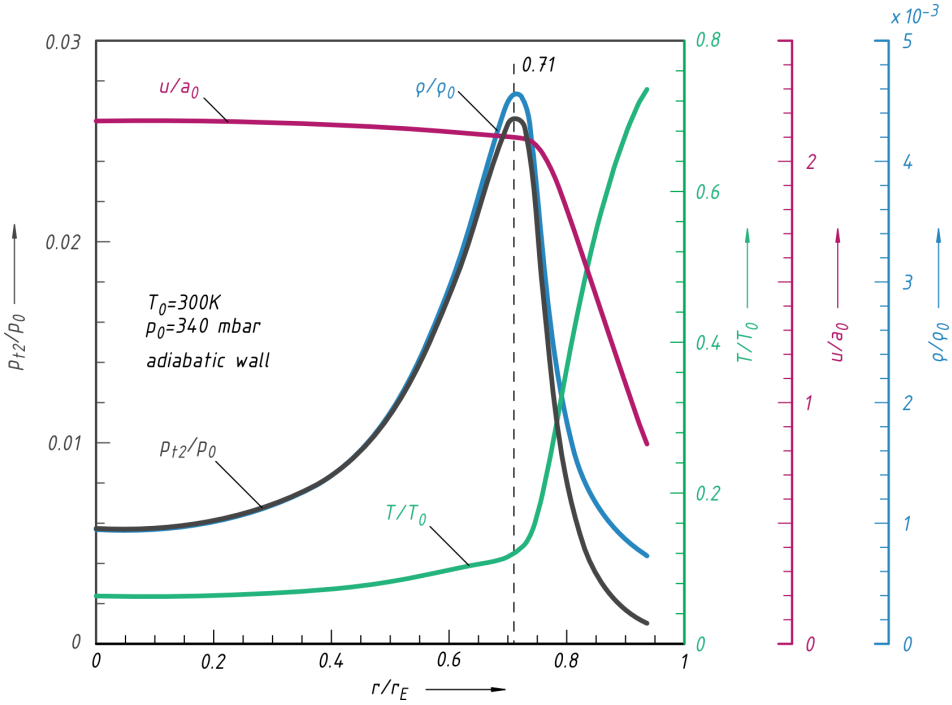

Figure 19: Calculated profiles at nozzle exit

4.3 Patterson-Probe

Besides analyzing nozzle and plume flow itself, numerical methods are also gainfully employed to help interpret the signals of measurement devices. Take for example the free-molecular impact pressure probe [Patterson, 1956], also known in the literature by the name “Patterson probe”.

The Patterson-probe is an instrument to measure particle flux in highly rarefied (free-molecular) flow. Knowledge of particle flux is the basis to properly estimate plume impingement effects. A reliable determination of particle flux will yield more accurate prediction of plume impingement effects.

Geometrically, the Patterson probe essentially is a cavity with an orifice. Actual probes for use in experimental facilities typically come in the shape of a hollow cylinder which is closed at one end. The other end is attached to a pressure gauge suitable for high vacuum. To minimize the influence of walls on the entering flow, the probe orifice is located on the longitudinal side of the cylinder (conveniently placed near the closed end). The length of the channel between ambient and internal flow is thus reduced to approximately the wall thickness of the cylinder. Consequently, the probe cylinder is placed perpendicular to the flow.

The measured quantities are: pressure p_K and temperature T_K at the gauge, and temperature T_2 at the tip (closed end) of the probe. From these, one infers the pressure p_2 at the tip of the probe from Knudsen’s thermal transpiration relation (see also

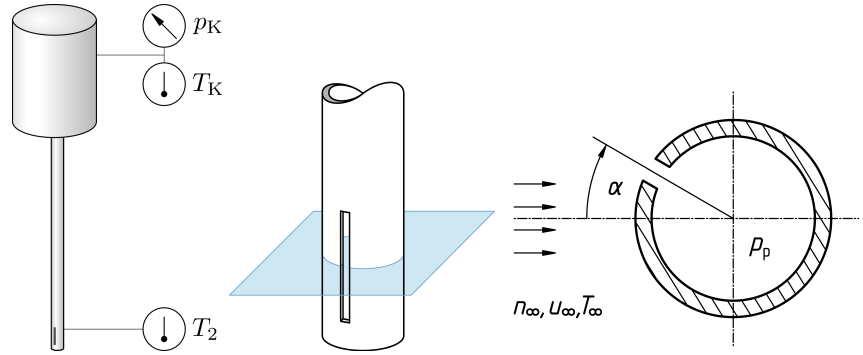

(a) Sketch of a Patterson probe

(b) Enlargement of probe head

Figure 20: The free-molecular impact pressure probe with slotted orifice, as proposed by Koppenwallner [Koppenwallner, 1984]

Fig. 20a)

$$\frac{p_2}{p_K} = \sqrt{\frac{T_2}{T_K}}. \tag{10}$$

4.3.1 Ideal Patterson probe

The concept of the free-molecular pressure probe is best explained in its ideal representation, i. e. neglecting wall thickness and finite orifice width. In the absence of intermolecular collisions, we can clearly distinguish two non-interfering fluxes at the orifice, one of the entering molecules and one of the particles effusing from within the probe. It is an obvious requirement that the two fluxes must be equal in steady state. If we denote by $\dot{n}_{\infty,\mathrm{p}}$ the number of particles per unit time per unit area that *enter* the probe:

$$\dot{n}_{\infty,\mathrm{p}} \stackrel{!}{=} \dot{n}_{\mathrm{p},\infty}, \tag{11}$$

$$\chi\left(S_\mathrm{n}\right) \cdot n_\infty \tilde{c}_\infty = n_\mathrm{p} \tilde{c}_\mathrm{p}, \tag{12}$$

where

$$\chi\left(S_\mathrm{n}\right) = \exp\left(-S_\mathrm{n}^2\right) + \sqrt{\pi} S_\mathrm{n} \left(1 + \mathrm{erf}\left(S_\mathrm{n}\right)\right) \tag{13}$$

is the well-known equilibrium flux function, that arises from integrating the equilibrium velocity distribution function over the half-space of velocities with a component pointing towards the probe entrance. It depends only on the molecular speed ratio S_n perpendicular to the entrance plane:

$$S_\mathrm{n} = \frac{u_\mathrm{n}}{\tilde{c}_\infty}. \tag{14}$$

The quantity $\tilde{c}$ in Eqs. (12, 14) designates the most probable thermal speed in equilibrium, it is directly proportional to the square-root of temperature and otherwise only

depends on the gas species. That said, Eq. (12) may be expressed as:

$$\left(\frac{n_2 T_2}{n_\infty T_\infty}\right)_{\mathrm{id}} = \left(\frac{p_2}{p_\infty}\right)_{\mathrm{id}} = \sqrt{\frac{T_2}{T_\infty}} \cdot \chi\left(S_{\mathrm{n}}\right), \tag{15}$$

where the subscript "id" refers to the "ideal" probe.

The actual number flux $\dot{n}_\infty$ is then computed from equating with the impingement rate of the gas trapped inside the probe (assumed to be in equilibrium):

$$\dot{n}_\infty = \dot{n}_{\mathrm{p}} = \frac{p_{\mathrm{p}}}{m\sqrt{\pi}\tilde{c}_{\mathrm{p}}}, \tag{16}$$

where m is the mass of one gas molecule.

4.3.2 Real Patterson probe

Real Patterson probes however exhibit non-ideal orifices and the finite wall thicknesses have an impact on the so-called transmission probability, i.e. the probability for a particle that crosses the entrance plane to eventually reach the exit plane of the orifice channel. The ratio of transmission probabilities Φ for particles leaving to particles entering the cavity is used as a factor to correct the theoretical particle flux of an ideal probe that would be computed from the actual pressure and temperature readings of the cavity.

This ratio of transmission probabilities is a function of free-stream (molecular) Mach-number S_∞, probe angle-of-attack α and geometry of the orifice (in this case the geometry is characterized by the channel aspect ratio Λ). It can easily be shown to equal the ratio of pressure in the ideal probe to the pressure in the real probe:

$$\dot{n}_\infty = \frac{P_{\mathrm{p},\infty}}{P_{\infty,\mathrm{p}}} \cdot \dot{n}_{\mathrm{p}}, \tag{17}$$

$$= \Phi \cdot \dot{n}_{\mathrm{p}}, \tag{18}$$

$$\Phi\left(S, \alpha, \Lambda\right) = \frac{\left(p_{\mathrm{p}}\right)_{\mathrm{id}}}{p_{\mathrm{p}}}. \tag{19}$$

Knowledge of Φ then allows to determine the actual number flux of the free stream particles through Eq. (18) and the flux of particles effusing from the probe, $\dot{n}_{\mathrm{p}}$, as calculated from Eq. 16.

Expressions (15, 19) may be used to compute the ratio of probabilities with numerical methods applicable to rarefied flow. It is thus possible to study the probe response (and sensitivity) for varying free-stream conditions and help interpret the probe signal.

Exemplary results of flow-field computations in and around the DLR Patterson-probe are presented in Fig. 21 for both highly rarefied (free molecular) and near-continuum flow. Both solutions were obtained with the DSMC method. The isopycnics in Fig. 21a nicely exhibit features of highly rarefied hypersonic flow, namely the drop-shadow-like wake region behind the cylinder and the absence of a shock in front of the probe.

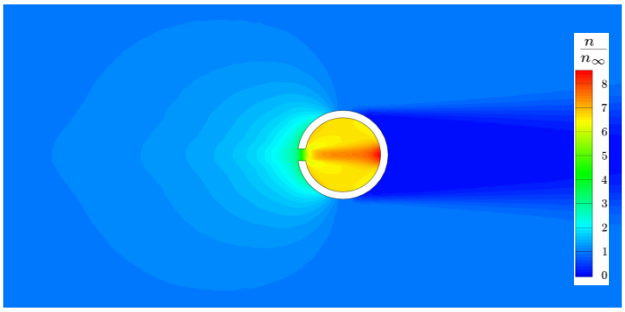

(a) Highly rarefied flow: $Kn_{\infty,\mathrm{p}} \approx 300$

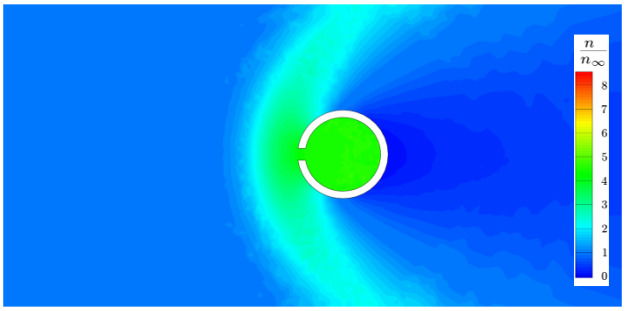

(b) Weakly rarefied flow: $Kn_{\infty,\mathrm{p}} \approx 0.3$

Figure 21: Contour plot of number density ratio n/n_∞ in and around a Patterson-probe, computed with DSMC ($S_\infty = 10$)

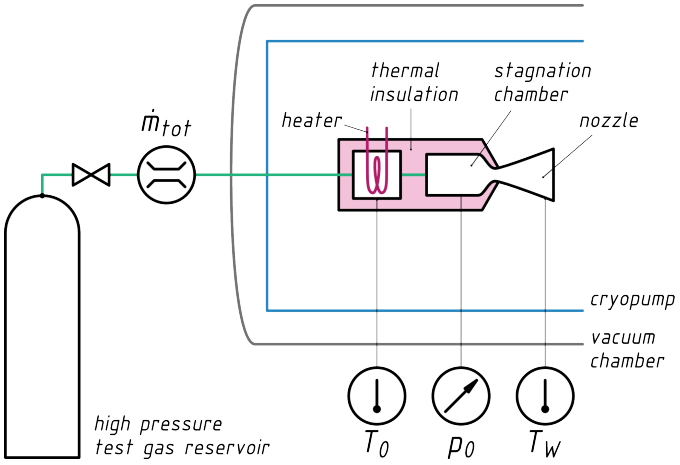

Figure 22: Simulated plume test setup (STG)

Entering molecules pass the orifice region as an undisturbed beam to impinge on the rear wall of the probe, only to be fully accommodated and scattered around in the probe cavity. The contribution of the effusing particles is clearly visible in the density contours in front of the orifice. To compute the ratio of transmission probabilities required to determine the correct number flux, one would establish an average density ratio n_2/n_∞ inside the cavity and employ Eqs. (15, 19).

With numerical methods such as DSMC it is possible to apply the same procedure to flowfields that are not free molecular. As the flow density increases, the impact of intermolecular collisions on the pressure inside the probe cavity will prevail over the influence of the probe and orifice walls. The parameter Φ, that relates actual free-stream particle flux to the value estimated from idealized free-molecular probe theory is then not a ratio of transmission probabilities in the classical sense. It may serve however to estimate the uncertainties to reckon with in off-design application of the probe in flow regimes that are not guaranteed to be free molecular and in which analytical determination of transmission probabilities is impossible.

4.4 Experimental results

In the following we exemplify some results. Some could only be obtained in space like vacuum (STG).

Molecule number flux measurements (note that the molecule number flux multiplied by the molecule mass yields the mass flux; both quantities are important to determine impingement effects) were carried out in so-called simulated plumes, i.e. the thrusters are operating with inert test gases instead of propellants. The advantage is a greater clarity in the initial experiments, since the values of the relevant parameters are known. Figure 22 shows a sketch of the setup. Stagnation pressure is adjusted via a mass flow controller, stagnation temperature may be increased by heating the stagnation

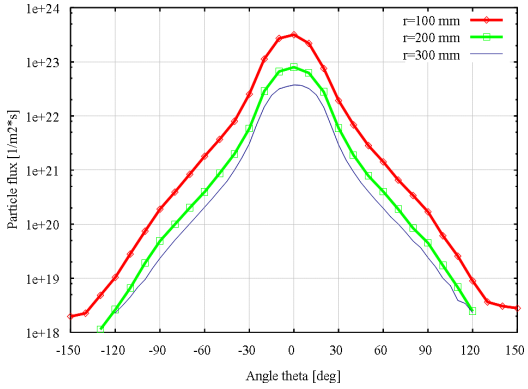

(a) Measured number flux at various distances from the nozzle exit

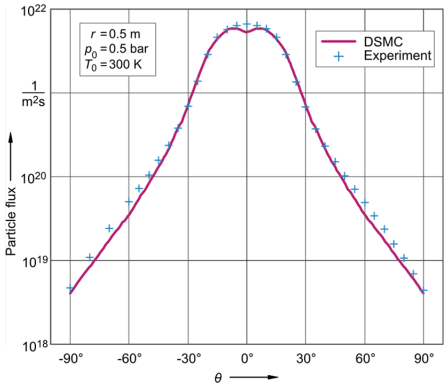

(b) Measured and computed number flux profiles

Figure 23: Angular number flux profiles of nitrogen cold-gas thrusters

chamber.

The diagram (Fig. 23a) shows an angular profile family of a plume emanating from a small cold-gas conical thruster nozzle. The impact of the guided expansion manifests itself through the noticable bulge from the axis up to an inflection point around 30^o. This domain of high number flux is the expanding nozzle core. The number flux beyond the inflection point is due to the expanding boundary layer. The three curves show data recorded at three different distances r from the nozzle exit. One can clearly see a fairly good self-similarity, which shows that the plume is indeed expanding radially even in the backflow $\theta > 90^o$, so the vacuum was sufficient to resemble space conditions.

Figure 23b shows a comparison of experimentally obtained particle flux data, plotted together with the results for a numerical computation of the same case. The computation was carried out with a DSMC code that used continuum CFD results as inflow boundary conditions. The whole flowfield was first computed with the continuum CFD code and a coupling interface along with the local boundary flux data was determined

from this solution. The flow was not everywhere supersonic perpendicular to the interface, and this manifests itself in the discrepancies observable for angles greater than 45^o. The dent in the DSMC result noticable at $\theta \approx 0^o$ is a well-known problem that may arise in simple axisymmetric implementations of the method due to too few particles in one DSMC cell near the axis.

5 Plume impingement analysis

Plume impingement effects can broadly be classified to be originating from mass flow (contamination), momentum flow (forces, moments) and energy (heat load). Quantifying the latter two requires knowledge of density ρ and speed u wich must be obtained from plume analysis. At least a coarse knowledge of the distribution of droplets is of course mandatory when a contamination analysis is to be carried out. In addition to a detailed knowledge about the plume shape, composition and flow field parameters, one also requires information about the location, extension and shape of the surface that is impinged.

Some methods to determine heat transfer and force in the context of plume impingement are already described in [Dettleff, 1991]. In this section we like to concentrate on two exemplary experiments related to plume impingement. The first subsection is concerned with pressure measurements on an impinged plate, while the second subsection describes investigations of so-called plume shields to reduce self-impingement due to backflow.

5.1 Pressure on a tangentially impinged plate

Here we will comment on the example of the tangentially impinged plate. A sketch of the plate and test setup is given in Fig. 24.

The plate was equipped for pressure measurements by drilling five holes on a line parallel to the plume axis and connected rearwards to pressure gauges. From the pressure the local force component perpendicular to the plate can be determined. The experiment was carried out in the CCG (see page 10) with a bipropellant thruster placed 50 mm from the plate.

The thruster was fired for 500 ms and the pressure signal on all five ports recorded, Fig. 25. Observe that a more or less constant pressure was reached at locations 2 to 5 after about 200 ms. The delayed response can here be attributed to the reaction time of the pressure gauges used in this investigation. At location 0 however, which is in the nozzle exit plane, the signal increases linearly, indicating an increase in *background gas pressure* during the firing time. Increase in background gas pressure is of course an effect induced by the (conventional) vacuum chamber and would not be observed in space. This shows again that great care must be taken while analyzing experimental results and to ensure that the simulation condition stayed adequate through the course of the experiment.

5.2 Reducing impingement effects

Reducing the generally adverse effects of plume impingement is an important objective in spacecraft design. Note that plume impingement will always have to be reckoned with, as the tendency of a gas jet to expand in all directions may be influenced by the design of the nozzle, but cannot be avoided.

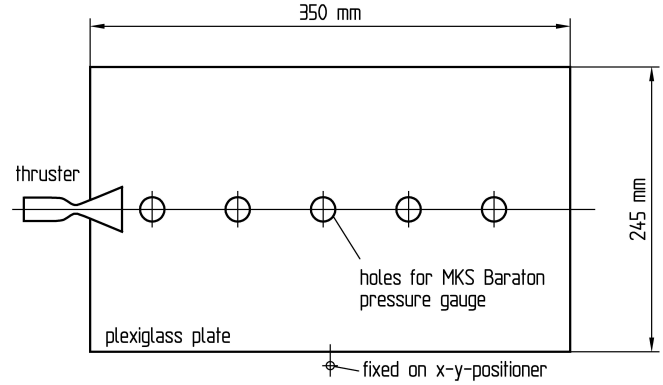

(a) side view

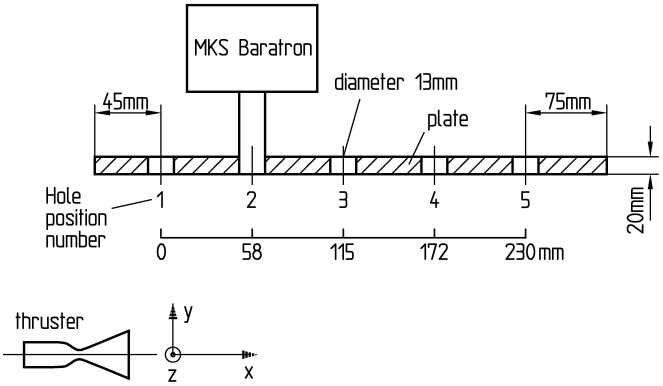

(b) top view showing loaction of pressure ports

Figure 24: Experimental setup for pressure measurement on a plate

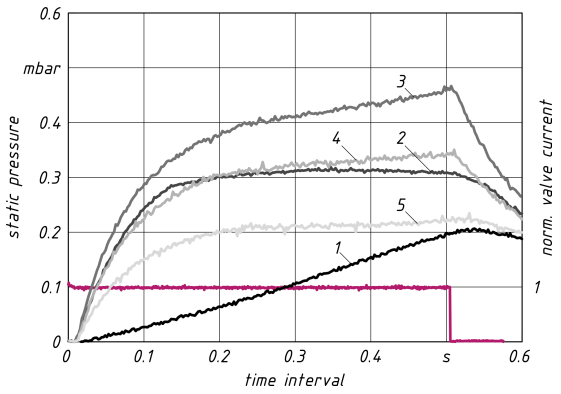

Figure 25: Pressure on the plate during thruster firing. Numbers 1 to 5 designate the positions of the pressure port, cf. Fig. 24

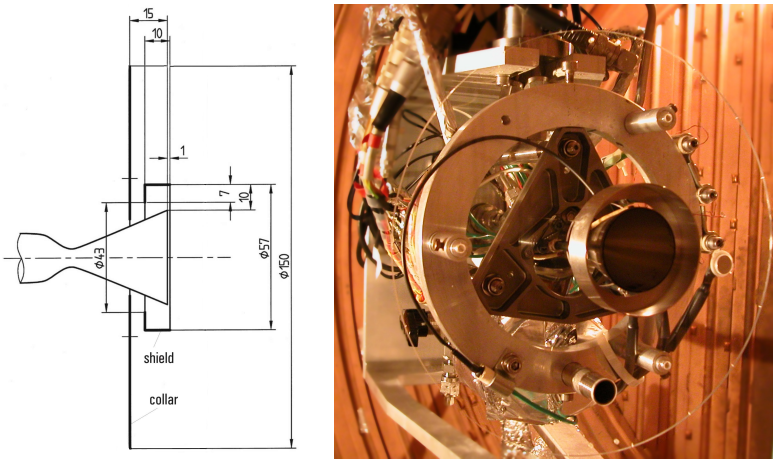

(a) Schematic

(b) Photograph of the plume shield and acrylic glass collar assembled to a 10 N bipropellant thruster

Figure 26: Installation of a plume shield to reduce backflow

The most straight-forward way of at least partially reducing the impingement onto certain surfaces is shielding. Recall the droplet contamination of a surface immediatly upsteam of the nozzle exit plane of a bipropellant thruster, as described previously (Fig. 11 on page 21). The droplets witnessed in this location originate from the cooling film which, due to its relatively low speed, expands into the backflow region of the nozzle, together with the gas from the nozzle boundary layer. In an attempt to protect the collar surface, a plume shield was constructed and installed (Fig. 26) to hinder the backflow.

After the test shield and collar where disassembled for closer inspection (Fig. 27). While clearly some non-evaporating liquid was collected by the shield, fine droplets are still visible on the collar. Full protection was thus not achieved.

The effectiveness of a plume shield to mitigate pure gas backflow was then investigated using a nitrogen cold gas thruster equipped with a plume shield. Angular profiles of the mass flux measured with a Patterson probe show that a local reduction of up to 50% is possible in the backflow regime (Fig. 28).

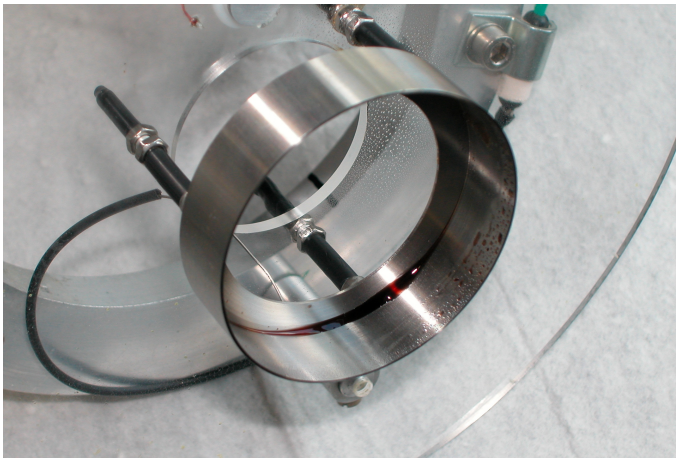

Figure 27: Plume shield and collar assembly after the experiment. Note the unburnt fuel gathered in the shield and the fine droplets on the acrylic glass collar

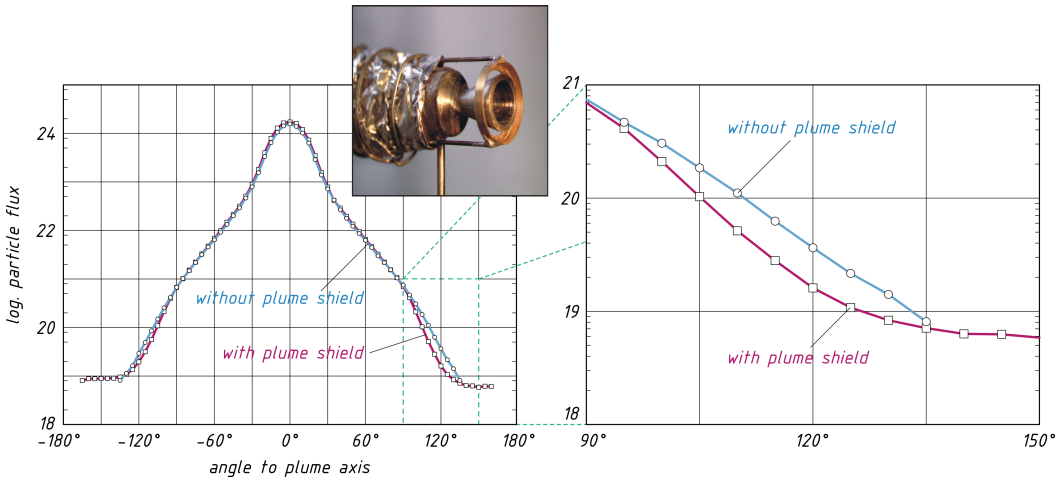

Figure 28: Effect of plume shield on the backflow of a cold gas thruster

6 Summary

Plume impingement from chemical and cold gas thrusters aboard space vehicles is an important phenomenon to reckon with, as the generally adverse impingement effects, such as contamination, forces and moments, as well as heat loads, can jeopardize the spacecraft's mission by shortening it's life time (excessive fuel consumption due to compensating unanticipated moments) or even rendering critical instrumentation useless, e. g. because of contamination of optical surfaces. Accounting for the effects of plume impingement in an early phase of mission and vehicle design is thus desirable, as it reduces the risk of economic or technical failure.

Prediction of plume impingement effects naturally requires a thorough understanding of the constituents and expansion behavior of an individual thrusters plume which is why research is performed on the subject for many decades now.

We have in this article introduced main features of plumes from chemical and cold gas thrusters and a selection of tools necessary to investigate them both numerically and experimentally. Exemplary results of plume structure and impingement effects are given. Careful checking and matching is required to eventually use these results to successfully predict plume impingement effects.

The brevity of this article only permits a presentation that is far from complete and we have restricted ourselves to merely touching on aspects that seem intuitive to grasp. We hope to have sufficiently stressed the point that a best possible understanding of exhaust plumes of chemical thrusters can only be attained by tight combination and improvement of experimental and numerical techniques - and a bit of experience.

References

[Anderson, 1995] Anderson, J. (1995). *Computational Fluid Dynamics*. 1st edition.

[Ashkenas and Sherman, 1966] Ashkenas, H. and Sherman, F. S. (1966). The structure and utilization of supersonic free jets in low density wind tunnels. In *Proceedings of the 5th International Symposium on Rarefied Gas Dynamics*, volume 2, pages 84–105, New York. Academic Press.

[Bird, 1970] Bird, G. A. (1970). Breakdown of translational and rotational equilibrium in gaseous expansions. *AIAA Journal*, 8(11):1998–2003.

[Bird, 1994] Bird, G. A. (1994). *Molecular Gas Dynamics and the Direct Simulation of Gas Flows*. Oxford University Press.

[Bird et al., 2009] Bird, G. A., Gallis, M. A., Torczynski, J. R., and Rader, D. J. (2009). Accuracy and efficiency of the sophisticated direct simulation monte carlo algorithm for simulating noncontinuum gas flows. *Physics of Fluids*, 21:017103, 1–12.

[Dettleff, 1991] Dettleff, G. (1991). Plume flow and plume impingement in space technology. *Progress in Aerospace Sciences*, 28(1):1–71.

[Driftmyer, 1972] Driftmyer, R. T. (1972). A correlation of freejet data. *AIAA Journal*, 10:1093–1095.

[Gallis et al., 2009] Gallis, M., Torczynski, J., Rader, D., and Bird, G. (2009). Convergence behavior of a new dsmc algorithm. *Journal of Computational Physics*, 228(12):4532 – 4548.

[Gatsonis et al., 1999] Gatsonis, N. A., Nanson, R. A., and LeBeau, G. J. (1999). Navier-stokes/DSMC simulations of cold-gas nozzle/plume flows and flight data comparisons. In *33rd Thermophysics Conference*, AIAA Paper 1999-3456, Norfolk, US-VA.

[Koppenwallner, 1984] Koppenwallner, G. (1984). The free molecular pressure probe with finite length slot orifice. In Oguchi, H., editor, *Rarefied Gas Dynamics*, number 14 in International Symposium on Rarefied Gas Dynamics, pages 415–422, Tsukuba. University of Tokyo Press.

[Lumpkin et al., 1995] Lumpkin, F. E., LeBeau, G. J., and Stuart, P. C. (1995). A cfd/DSMC analysis of plumes and plume impingement during shuttle/mir docking. In *30th AIAA Thermophysics Conference*, AIAA Paper 1995-2034, San Diego, US-CA.

[Lumpkin et al., 1996] Lumpkin, F. E., Stuart, P. C., and LeBeau, G. J. (1996). Enhanced analyses of plume impingement during shuttle-mir docking using a combined cfd and DSMC methodology. In *31st AIAA Thermophysics Conference*, AIAA Paper 1996-1877, New Orleans, US-LA.

[Papp et al., 2006] Papp, J. L., Wilmoth, R. G., Chartrand, C. C., and Dash, S. M. (2006). Simulation of high-altitude plume flow fields using a hybrid continuum cfd/DSMC approach. In *42nd AIAA/ASME/SAE/ASEE Joint Propulsion Conference and Exhibit*, Sacramento, CA.

[Patterson, 1956] Patterson, G. (1956). Theory of free-molecule orifice-type pressure probes in isentropic and non-isentropic flows. UTIAS Report 41, University of Toronto Institute for Aerospace Studies, Toronto.

[Smolderen, 1965] Smolderen, J. J. (1965). The evolution of the equations of gas flow at low density. In Küchemann, D. and Sterne, L. H. G., editors, *Progress in Aeronautical Sciences*, volume 6, pages 1–132. Pergamon Press.

[Traphan, 2011] Traphan, D. (2011). Experimentelle Untersuchung von Freistrahlen aus geometrisch ähnlichen Düsen. Master's thesis, Georg-August-Universität Göttingen.

[Wang and Boyd, 2002] Wang, W.-L. and Boyd, I. D. (2002). Continuum breakdown in hypsersonic viscous flows. In *40th AIAA Aerospace Sciences Meeting and Exhibit*, AIAA Paper 2002-0651, Reno, US-NV.